Available online at www.eccomasproceedia.org
Eccomas Proceedia SMART (2023) 158-168

ECCOMAS
Proceedia

X ECCOMAS Thematic Conference on Smart Structures and Materials
SMART 2023
D.A. Saravanos, A. Benjeddou, N. Chrysochoidis and T. Theodosiou (Eds)

PROGRAMMABLE HARDENING, SOFTENING, AND ESSENTIALLY NONLINEAR SYNTHETIC INDUCTANCE-BASED PIEZOELECTRIC SHUNT CIRCUITS

OBAIDULLAH ALFAHMI* **AND ALPER ERTURK***

* G.W. Woodruff School of Mechanical Engineering
Georgia Institute of Technology
Atlanta, GA, 30332, USA

Abstract. Piezoelectric shunt damping techniques have been extensively studied over the past several decades for vibration attenuation in light-weight structures. The existing piezoelectric shunt damping techniques have been mostly limited to linear or switching nonlinear circuits, with the exception of a few nonlinear capacitance efforts. Through nonlinear synthetic impedance circuitry, this work first introduces cubic inductance to emulate Duffing-type hardening and softening nonlinearity in the shunt circuit with precise programming and tuning capability through digital control. The shunt circuit comprises linear inductance, linear resistance, and cubic inductance, all enabled by synthetic impedance and connected in parallel with each other and to the piezoelectric element's inherent capacitance to create a Duffing circuit. Both hardening and softening inductance cases are studied for different nonlinear coefficients and excitation amplitudes. In the second part, the linear inductance is removed in the hardening case to create a nonlinear energy sink behavior through the essential nonlinearity (without requiring negative capacitance unlike the existing efforts). Experiments are conducted on a piezoelectric bimorph cantilever under base excitation for concept demonstration and model validation. First, linear frequency response functions of the cantilever are obtained for the short- and open-circuit conditions, and for linear resistive-inductive synthetic shunt damping, to confirm the standard linear behavior and electromechanical model parameters. Then, cubic inductance is introduced to the circuit and nonlinear experiments (up- and down-frequency sweep) are conducted for the hardening and softening Duffing circuit scenarios. Linear inductance is then removed in the experiments to enable essentially nonlinear circuit in the hardening case. Structural resonance is modified (by means of a tip mass) in the nonlinear energy sink case to demonstrate wideband absorption capability without tuning the circuit parameters. Experimental results agree well with the numerical simulations for this family of nonlinear synthetic impedance circuits.

Key words: Nonlinearity, synthetic impedance, piezoelectric shunt damping

Peer-review under responsibility of the organizing committee of SMART 2023.
doi: 10.7712/150123.9774.445829

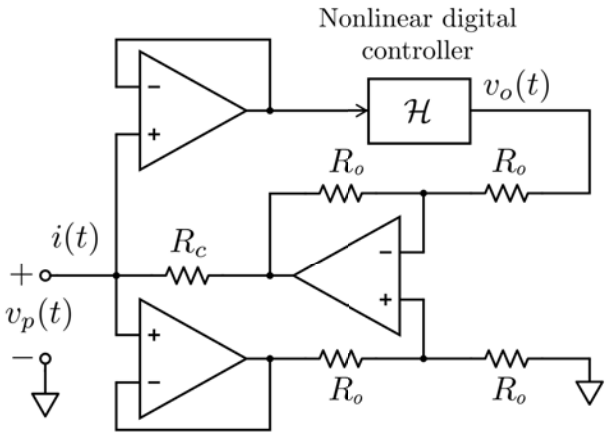

Figure 1: Howland current pump-based synthetic impedance circuit with a nonlinear digital controller.

1 INTRODUCTION

Intentionally designed nonlinearities have drawn great attention in the field of vibration isolation and absorption due to the significant improvement in bandwidth and performance obtained from the introduction of such nonlinearities [1, 2, 3, 4, 5, 6, 7]. In this paper, we propose a novel approach for emulating the impedance of hardening- and softening-type Duffing nonlinearities, followed by a nonlinear energy sink (NES) with essential nonlinearity using digitally programmable synthetic nonlinear inductance. The performance of these digital nonlinear shunts is analyzed and experimentally validated for various cases of excitation amplitudes and frequencies. For the standard hardening/softening Duffing shunt case, several nonlinear coefficients are explored. In the NES case, the primary structure is modified by changing the tip mass while keeping the shunt parameters unchanged to ensure the robustness of the absorber in allowing for irreversible energy transfer from the host structure to the nonlinear attachment. A key advantage of NES is that it can absorb vibrations over a wide frequency bandwidth without the need for tuning in the absence of a preferential linear resonance. It is noteworthy that, to date, piezoelectric NES has only been demonstrated using circuits (mostly analog) that incorporate nonlinear capacitance, which necessitates the use of negative capacitance to create essential nonlinearity [8]. In contrast, our approach is based on inductance and does not require negative capacitance.

2 GOVERNING NONLINEAR EQUATIONS

Synthetic impedance is a voltage-controlled current source that can be employed to emulate arbitrary circuit elements [9]. Figure 1 illustrates the circuit diagram of a Howland current pump-based synthetic impedance circuit with a nonlinear digital controller.

The current output from the synthetic impedance circuit $i(t)$ is determined by the piezoelec-

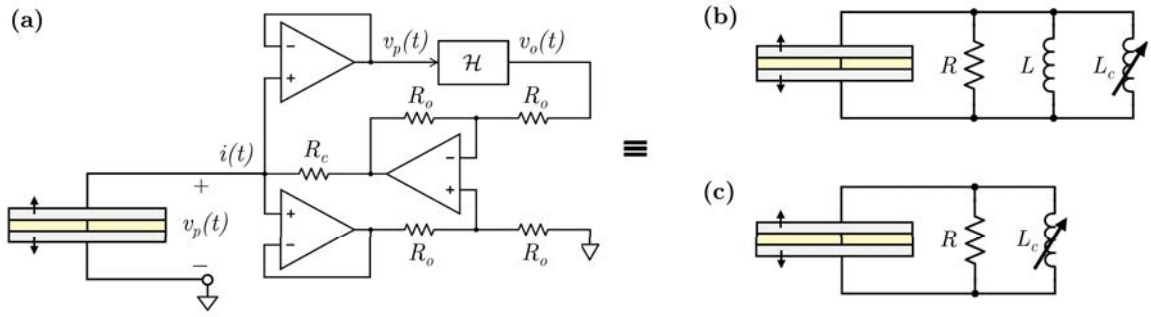

Figure 2: (a) Schematic of the bimorph piezoelectric structure shunted to the synthetic impedance circuit which can emulate arbitrary circuits such as (b) linear resistor, linear inductor, and nonlinear cubic inductor in parallel connection to give a Duffing oscillator, and (c) nonlinear energy sink with essential nonlinearity with no linear resonance in the circuit.

tric voltage input:

$$i(t) = \frac{v_o(t)}{R_c} = \frac{\mathcal{H}\{v_p(t)\}}{R_c} \tag{1}$$

where R_c is a reference resistance in the circuit and $v_o(t) = \mathcal{H}\{v_p(t)\}$ is the output voltage from the controller, calculated as a nonlinear integro-differential operator $\mathcal{H}$ acting on the measured piezoelectric voltage $v_p(t)$.

In this work, we employ the synthetic impedance circuit to emulate two different digital shunts (hardening/softening Duffing and NES) as illustrated in Figure 2. For the Duffing oscillator case, the circuit operator $\mathcal{H}$ takes the form

$$\mathcal{H}\{v_p(t)\} = K_p v_p(t) + K_i \int_0^t v_p(\tau)d\tau + K_c \left(\int_0^t v_p(\tau)d\tau \right)^3 \tag{2}$$

while for the NES case, it takes the form

$$\mathcal{H}\{v_p(t)\} = K_p v_p(t) + K_c \left(\int_0^t v_p(\tau)d\tau \right)^3 \tag{3}$$

Here, K_p is the proportional gain which represents a linear resistor, K_i is the integral gain for emulating a linear inductor, and K_c is the integral-cubic gain for obtaining the nonlinear cubic inductor. Hence, the emulated electrical components can be given by

$$R = \frac{R_c R_b}{K_p R_b + R_c}, \qquad L = \frac{R_c}{K_i}, \qquad L_c = \frac{R_c}{K_c} \tag{4}$$

Next, we proceed with the derivation of the Duffing case as it represents a more general form. Note that the NES case can be derived by simply eliminating the K_i term.

Substituting Eq. (2) into Eq. (1), the current supplied by the synthetic impedance circuit is eventually obtained as

$$i(t) = \frac{K_p}{R_c} v_p(t) + \frac{K_i}{R_c} \int_0^t v_p(\tau)d\tau + \frac{K_c}{R_c} \left(\int_0^t v_p(\tau)d\tau \right)^3 \tag{5}$$

Here, positive or negative values of K_c correspond to a hardening- or a softening-type Duffing shunt, respectively.

The structure shunted to the synthetic impedance circuit is a bimorph cantilevered beam which undergoes harmonic base excitation in the transverse direction of the beam. The symmetric piezoelectric layers are connected in series with opposite poling directions along the thickness of the piezoelectric layers. The piezoelectric layers are modeled as a current source (voltage-dependent current source due to two-way coupling) connected in parallel to its inherent capacitance.

The force balance and current balance equations of the system (the cantilevered piezoelectric structure shunted to the nonlinear Duffing oscillator) for vibrations around the first bending mode are then [7]

$$\frac{\mathrm{d}^2 w_{rel}(t)}{\mathrm{d}t^2} + 2\zeta_1\omega_1\frac{\mathrm{d}w_{rel}(t)}{\mathrm{d}t} + \omega_1^2 w_{rel}(t) - \phi_1\theta_1 v_p(t) = \phi_1 f_1(t) \tag{6}$$

$$C_p\frac{\mathrm{d}v_p(t)}{\mathrm{d}t} + \frac{\theta_1}{\phi_1}\frac{\mathrm{d}w_{rel}(t)}{\mathrm{d}t} + \frac{1}{R_b}v_p(t) + \frac{K_p}{R_c}v_p(t) + \frac{K_i}{R_c}\int_0^t v_p(\tau)d\tau + \frac{Kc}{R_c}\left(\int_0^t v_p(\tau)d\tau\right)^3 = 0 \tag{7}$$

where $w_{rel}(t)$ is the transverse displacement of the tip of the beam relative to the transverse base displacement $w_b(t)$; $v_p(t)$ is the voltage across the shunt circuit and R_b is the bias resistance used to dissipate DC bias current from the operational amplifiers. The expressions for the equivalent inherent capacitance of the two piezoelectric layers connected in series, C_p, the fundamental undamped natural frequency of the beam in short-circuit conditions, ω_1, the first bending mode's purely mechanical viscous damping ratio, ζ_1, the modal electromechanical coupling term, θ_1, the eigenfunction evaluated at the tip of the beam, ϕ_1, and the modal forcing due to base excitation, $f_1(t)$, can be found elsewhere [7, 10, 11].

Finally, the governing electromechanical equations can be rewritten in terms of the emulated electrical components, namely the linear resistor, R, the linear inductor, L, and the nonlinear cubic inductor, L_c, as follows

$$\frac{\mathrm{d}^2 w_{rel}(t)}{\mathrm{d}t^2} + 2\zeta_1\omega_1\frac{\mathrm{d}w_{rel}(t)}{\mathrm{d}t} + \omega_1^2 w_{rel}(t) - \phi_1\theta_1 v_p(t) = \phi_1 f_1(t) \tag{8}$$

$$C_p\frac{\mathrm{d}v_p(t)}{\mathrm{d}t} + \frac{\theta_1}{\phi_1}\frac{\mathrm{d}w_{rel}(t)}{\mathrm{d}t} + \frac{1}{R}v_p(t) + \frac{1}{L}\int_0^t v_p(\tau)d\tau + \frac{1}{L_c}\left(\int_0^t v_p(\tau)d\tau\right)^3 = 0 \tag{9}$$

3 EXPERIMENTAL SETUP

The practical realization of the programmable Duffing shunts and NES shunts are explored by combining the nonlinear synthetic impedance circuit with a bimorph cantilever. The experiments are run at range of frequencies around the first bending mode of the beam with suitable frequency sweep rates (3 Hz/min for the Duffing case and 10 Hz/min for the NES case). It is worth noting that in order to capture the typical bifurcation behaviour of a mechanical structure shunted to a Duffing oscillator, the experiments are conducted at a lower up and down frequency

sweep rate compared to the NES case. Also, in the Duffing case, the response of the system is obtained for various values of the integral-cubic gain K_c ($\pm 3 \times 10^5, \pm 4 \times 10^5, \pm 5 \times 10^5$, and $\pm 6 \times 10^5$ [ΩH^{-3}]) and several root-mean-square (RMS) values of the base acceleration amplitudes (15, 20, 25 and 30 mg, where g is the gravitational acceleration). Nonlinear frequency response curves of the system (namely the vibration transmissibility and voltage per base acceleration) are obtained to evaluate the capability of the synthetic impedance circuit in emulating hardening and softening oscillators and ensure the fidelity of the nonlinear electromechanical model.

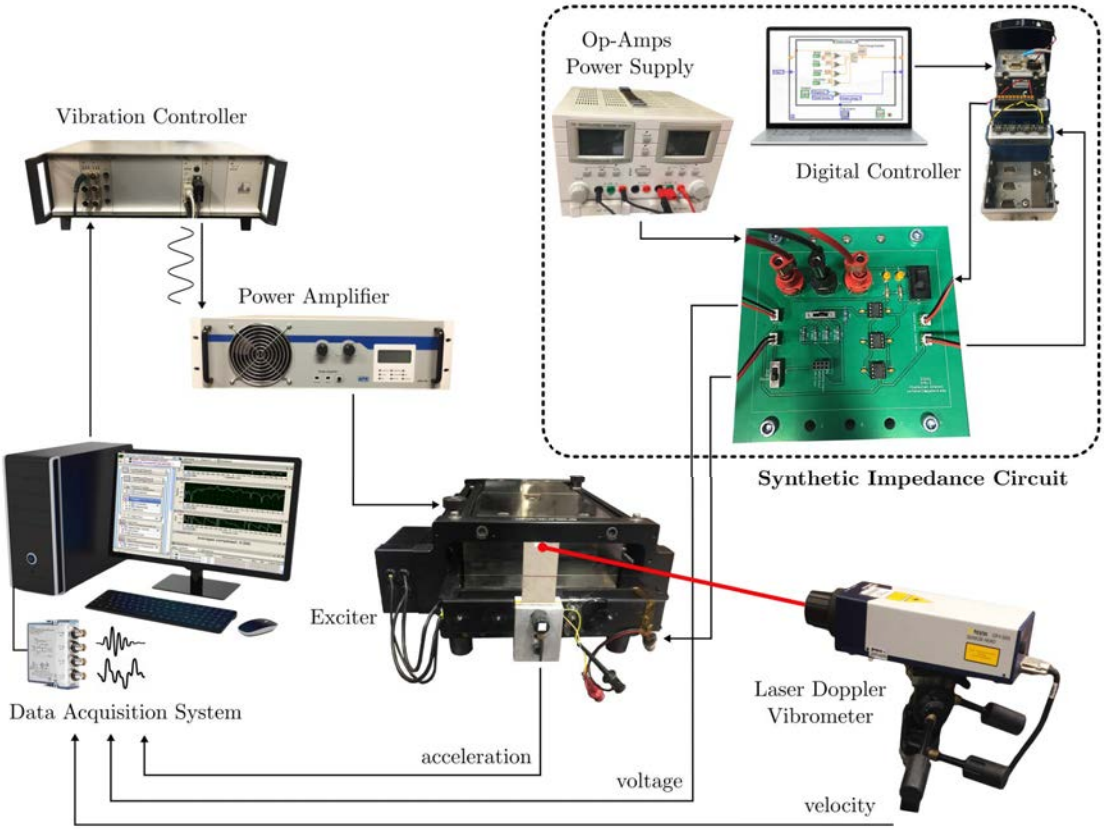

Figure 3: An overview of the experimental setup. The bimorph piezoelectric cantilever is shunted to the synthetic impedance circuit. The base acceleration, the tip velocity, and the piezoelectric voltage are continuously measured to obtain the frequency response curves of the system

In order to explore the robustness of the programmable piezoelectric NES, different structures are considered by changing the tip mass values (M_t = 0, 0.5 or 1 g), while the shunt circuit parameters are kept the same for all cases ($K_p = 0.25$ and $K_c = 7 \times 10^7 \Omega H^{-3}$). Two RMS values of the base acceleration are considered here as well(10 mg and 30 mg). An overview of the experimental setup is shown in Figure. 3. The bimorph beam is fixed in a vertical position to the armature of an electrodynamic exciter that is driven by a power amplifier. An accelerometer

is used to measure the base acceleration, while a laser Doppler vibrometer is used to measure the transverse velocity of the beam tip. The voltage across the piezoelectric electrodes is measured directly from the beam. To keep a constant RMS value of acceleration levels, the shaker is controlled using a vibration controller that employs feedback from the accelerometer.

4 RESULTS AND DISCUSSIONS

The system responses for the Duffing case considering different mechanical base excitation amplitudes and nonlinearity coefficients are shown in Figure 4 through Figure 7. In both hardening and softening cases, the resonances are significantly distorted due to the cubic nonlinearity. The second mode exhibits a substantially wider bandwidth with the hardening nonlinearity, while the first mode has a wider bandwidth in the softening scenario. Overall, the voltage and transmissibility frequency response curves of the system demonstrate a high degree of agreement between the model simulations, and the experimental results, across a range of Duffing shunts (cubic coefficients) and excitation amplitudes.

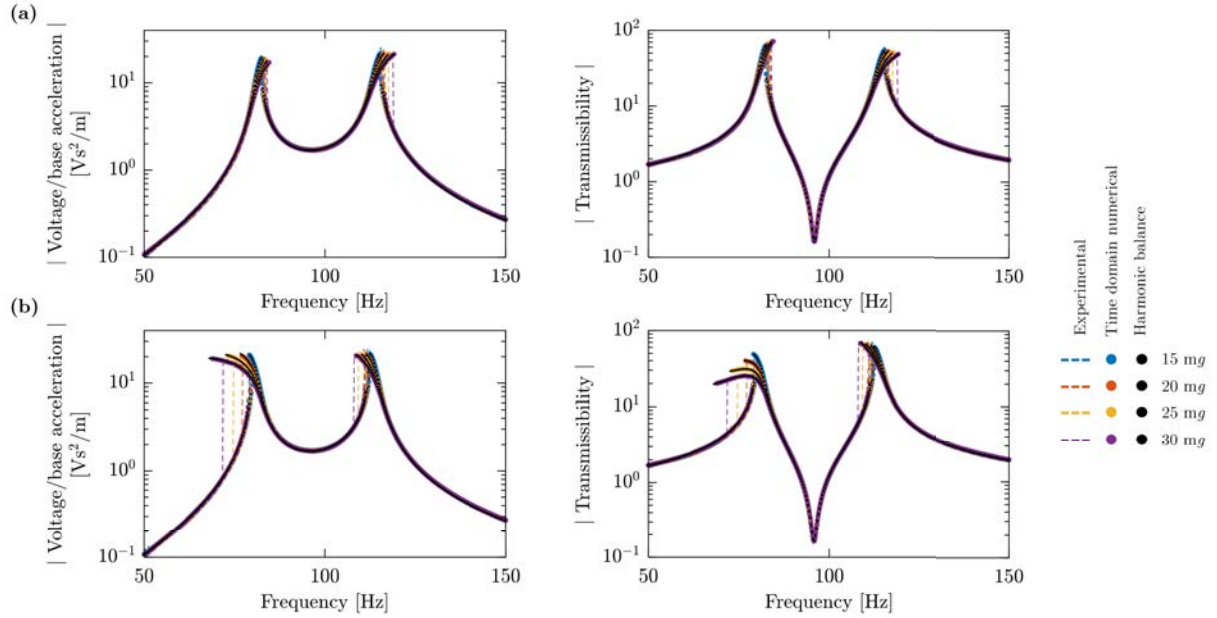

Figure 4: Voltage and transmissibility frequency response curves (in magnitude form) of the cantilevered beam shunted to (a) hardening-type Duffing circuit with $K_c = 3 \times 10^5\ \Omega\mathrm{H}^{-3}$ or (b) softening-type Duffing circuit with $K_c = -3 \times 10^5\ \Omega\mathrm{H}^{-3}$.

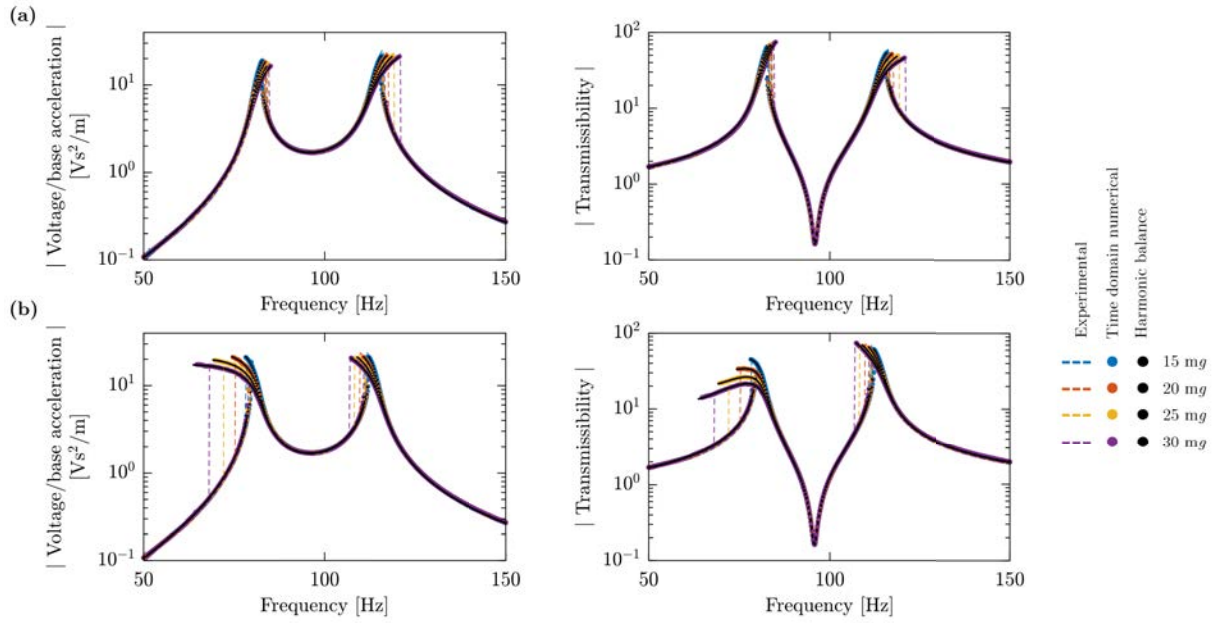

Figure 5: Voltage and transmissibility frequency response curves (in magnitude form) of the cantilevered beam shunted to (a) hardening-type Duffing circuit with $K_c = 4 \times 10^5\ \Omega\mathrm{H}^{-3}$ or (b) softening-type Duffing circuit with $K_c = -4 \times 10^5\ \Omega\mathrm{H}^{-3}$.

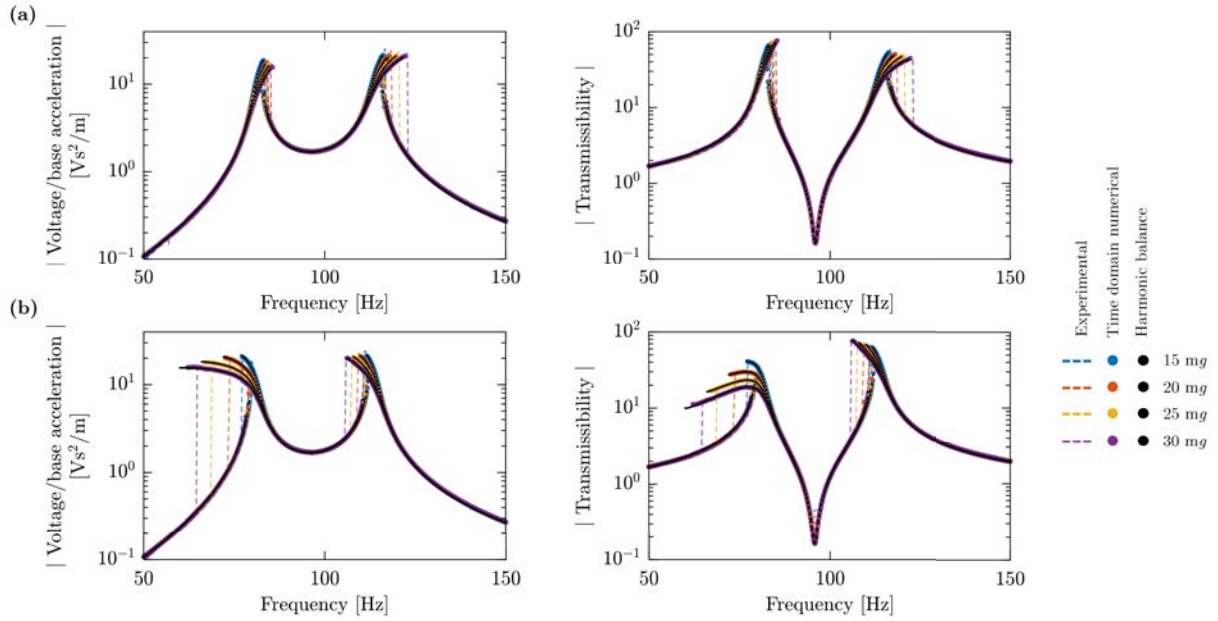

Figure 6: Voltage and transmissibility frequency response curves (in magnitude form) of the cantilevered beam shunted to (a) hardening-type Duffing circuit with $K_c = 5 \times 10^5\ \Omega\mathrm{H}^{-3}$ or (b) softening-type Duffing circuit with $K_c = -5 \times 10^5\ \Omega\mathrm{H}^{-3}$.

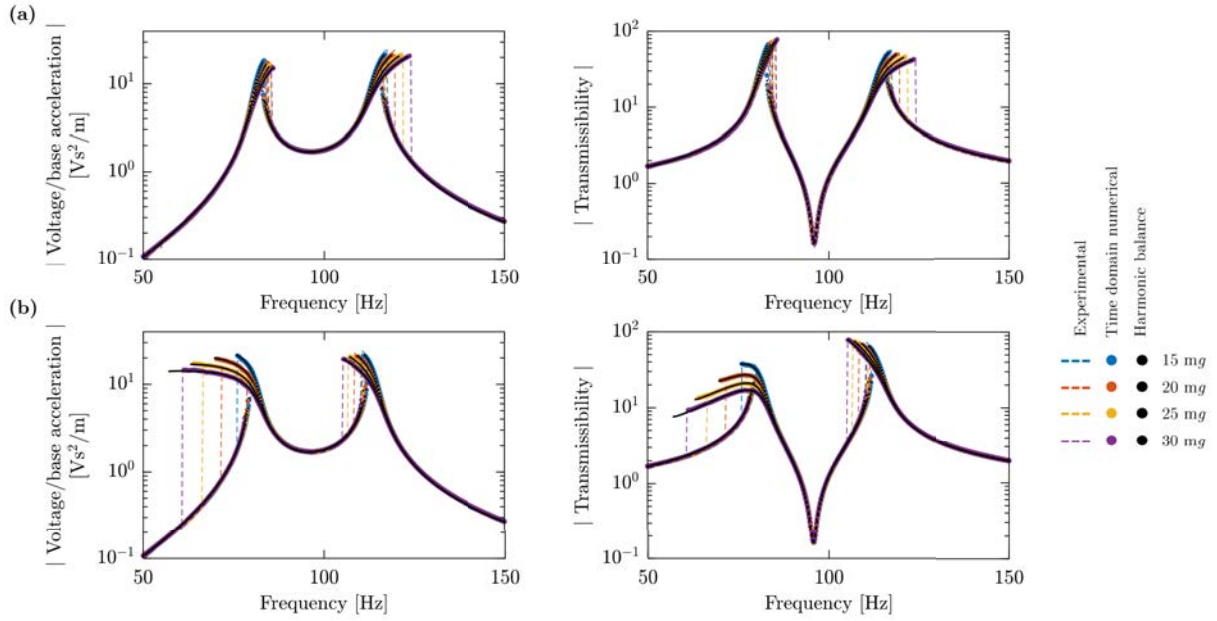

Figure 7: Voltage and transmissibility frequency response curves (in magnitude form) of the cantilevered beam shunted to (a) hardening-type Duffing circuit with $K_c = 6 \times 10^5\ \Omega\text{H}^{-3}$ or (b) softening-type Duffing circuit with $K_c = -6 \times 10^5\ \Omega\text{H}^{-3}$.

For the NES case, the experimental transmissibility frequency response is compared against numerical simulations, and the results are shown in Figures 8 and 9 for base accelerations of 10 mg and 30 mg, respectively. The transmissibility is analyzed for three different tip mass values, namely 0 g, 0.5 g, and 1 g. It is observed that the transmissibility of the shunted system is significantly reduced, ranging from 80% to 90%, in comparison to the short-circuit or open-circuit cases. This finding indicates that the synthetic impedance-based NES functions effectively, even when the system is altered. Additionally, the level of attenuation is seen to increase with greater excitation amplitudes, as expected. Furthermore, the experimental results are in good agreement with the numerical simulations, indicating the validity of the model.

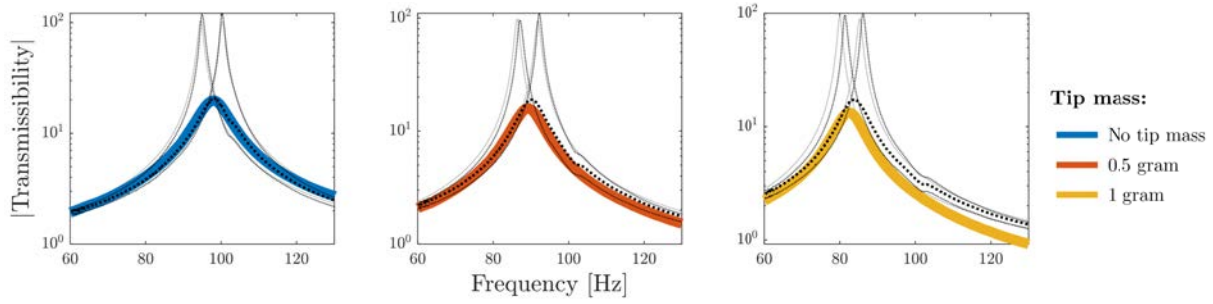

Figure 8: Transmissibility frequency response curves for the beam under harmonic base excitation of 10 mg, for three different tip mass cases. The continuous lines express the model simulation results while the experimental results are illustrated by dotted lines.

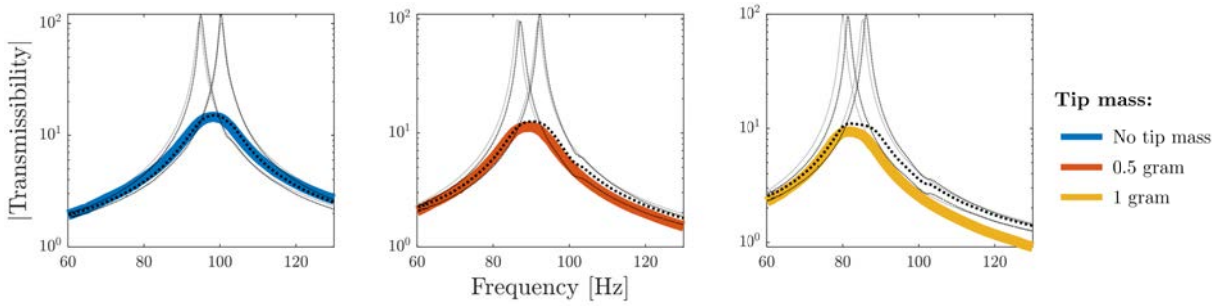

Figure 9: Transmissibility frequency response curves for the beam under harmonic base excitation of 30 mg, for three different tip mass cases. The continuous lines express the model simulation results while the experimental results are illustrated by dotted lines.

5 CONCLUSIONS

This work demonstrates the use of programmable nonlinear synthetic impedance circuits in emulating Duffing shunts with hardening or softening nonlinearities as well as a nonlinear energy sink (NES) with essential nonlinearity. A bimorph piezoelectric cantilever under harmonic base excitation is shunted to the synthetic impedance circuit in both cases. The model results are validated experimentally for various mechanical excitation amplitudes and frequencies considering several nonlinear coefficients in the Duffing case and modified primary structures for the NES case. The resonances of the nonlinear electromechanical system are significantly altered and attenuated due to the cubic nonlinearity of the digital Duffing oscillator without affecting the anti-resonance resulting from the linear inductance. The NES case, on the other hand, has shown significant vibration attenuation for a wide range of frequencies, considering different tip mass values, which indicates its robust operation, as expected. Overall, the results show a very good agreement between simulations and experimental results.

6 ACKNOWLEDGMENTS

Support from the Woodruff Professorship and the Carl Ring Family Chair funds is gratefully acknowledged.

REFERENCES

[1] K. Yang, R. Harne, K. Wang, and H. Huang, "Investigation of a bistable dual-stage vibration isolator under harmonic excitation," *Smart materials and structures*, vol. 23, no. 4, p. 045033, 2014.

[2] F. Romeo, G. Sigalov, L. A. Bergman, and A. F. Vakakis, "Dynamics of a linear oscillator coupled to a bistable light attachment: numerical study," *Journal of Computational and Nonlinear Dynamics*, vol. 10, no. 1, 2015.

[3] L. Li and P. Cui, "Novel design approach of a nonlinear tuned mass damper with duffing stiffness," *Journal of Engineering Mechanics*, vol. 143, no. 4, p. 04017004, 2017.

[4] P. Soltani and G. Kerschen, "The nonlinear piezoelectric tuned vibration absorber," *Smart Materials and Structures*, vol. 24, no. 7, p. 075015, 2015.

[5] B. Zhou, F. Thouverez, and D. Lenoir, "Essentially nonlinear piezoelectric shunt circuits applied to mistuned bladed disks," *Journal of Sound and Vibration*, vol. 333, no. 9, pp. 2520–2542, 2014.

[6] G. Raze, A. Jadoul, S. Guichaux, V. Broun, and G. Kerschen, "A digital nonlinear piezoelectric tuned vibration absorber," *Smart Materials and Structures*, vol. 29, no. 1, p. 015007, 2019.

[7] O. Alfahmi, C. Sugino, and A. Erturk, "Duffing-type digitally programmable nonlinear synthetic inductance for piezoelectric structures," *Smart Materials and Structures*, vol. 31, no. 9, p. 095044, 2022.

[8] T. M. Silva, M. A. Clementino, C. De Marqui Jr, and A. Erturk, "An experimentally validated piezoelectric nonlinear energy sink for wideband vibration attenuation," *Journal of Sound and Vibration*, vol. 437, pp. 68–78, 2018.

[9] A. Fleming, S. Behrens, and S. Moheimani, "Synthetic impedance for implementation of piezoelectric shunt-damping circuits," *Electronics Letters*, vol. 36, no. 18, pp. 1525–1526, 2000.

[10] A. Erturk and D. J. Inman, "An experimentally validated bimorph cantilever model for piezoelectric energy harvesting from base excitations," *Smart materials and structures*, vol. 18, no. 2, p. 025009, 2009.

[11] ——, *Piezoelectric energy harvesting*. John Wiley & Sons, 2011.